PHYSICAL REVIEW D **80,** 065018 (2009)

Computing the Casimir energy using the point-matching method

F. C. Lombardo,[1,*] F. D. Mazzitelli,[1,†] M. Vázquez,[2,‡] and P. I. Villar[1,2,§]

[1]*Departamento de Física Juan José Giambiagi, FCEyN University of Buenos Aires, Facultad de Ciencias Exactas y Naturales, Ciudad Universitaria, Pabellón I, 1428 Buenos Aires, Argentina*

[2]*Computer Applications on Science and Engineering Department, Barcelona Supercomputing Center (BSC), 29, Jordi Girona 08034 Barcelona, Spain*

(Received 19 August 2009; published 18 September 2009)

We use a point-matching approach to numerically compute the Casimir interaction energy for a two perfect-conductor waveguide of arbitrary section. We present the method and describe the procedure used to obtain the numerical results. At first, our technique is tested for geometries with known solutions, such as concentric and eccentric cylinders. Then, we apply the point-matching technique to compute the Casimir interaction energy for new geometries such as concentric corrugated cylinders and cylinders inside conductors with focal lines.

DOI: 10.1103/PhysRevD.80.065018 PACS numbers: 12.20.Ds, 03.70.+k, 11.10.−z

I. INTRODUCTION

One of the most clear macroscopic manifestations of quantum mechanics is the Casimir force [1]: a tiny force, relevant at short distances, which appears on uncharged bodies due to changes in the zero-point energy associated to quantum vacuum fluctuations. Quantum effects like Casimir forces have become increasingly important as electronic and mechanical systems on the nanometer scale become more prevalent. In the last 10 years, Casimir-force measurements have been made in a wide variety of experiments, for example, plate-plate [2], sphere-plate [3], and crossed cylinders [4] configurations. There are also proposals for measuring the Casimir force in the cylinder-plane configuration [5]. A recent experiment [6] implies that Casimir interactions are relevant in the fabrication of commercially micro-electro-mechanical systems devices. Techniques for predicting Casimir forces in general geometries are clearly needed if theory is to keep pace with the flourishing of experimental Casimir data and the design challenges of future micro-electro-mechanical systems devices.

In this framework, accurate modeling of Casimir forces in general geometries and for arbitrary electromagnetic properties of the uncharged bodies becomes very important. Shape and geometry can strongly influence the Casimir interactions. Several theoretical techniques have been developed in order to understand the geometric dependence of the Casimir force. These include the use of the argument theorem to perform explicitly the sum over modes [7–10], semiclassical and optical approximations [11], methods based on functional integrals [12], and scattering theory [13]. Many of these approaches have a common root in the multiple scattering theory developed in the seventies [14] (see also [15] for an updated review and applications to semitransparent bodies), and the evolution in the computational power allowed a precise numerical evaluation that involves, in general, the computation of determinants of infinite matrices.

There are also full numerical approaches, as the worldline numerics [16], that has been applied to scalar fields satisfying Dirichlet boundary conditions, or finite difference methods that evaluate the Casimir energy from the two-point function of the electromagnetic field [17]. As a consequence of this theoretical activity, we now have exact results for a variety of geometries that involve perfectly conducting shells: cylinder and sphere in front of a plane [18–20], eccentric cylinders [9,10,21], two-spheres [19,22], surfaces with periodic corrugations [23], Casimir pistons [24], multibody interactions involving plates and cylinders [25] or squares [17], objects of spheroidal or nearly-spheroidal shape [26], etc. Some of these methods also apply to the case of imperfect mirrors.

The Casimir force between two conductor bodies with simple shapes is in general attractive and monotonically decreasing with the separation among conductors. Thus, one might ask whether complex geometries might give rise to unexpected phenomena, such as nonmonotonic forces. For more complicated geometries, however, full numerical calculations become extremely difficult and therefore it is worth analyzing alternative approaches.

In this paper, we explore a new numerical approach to compute the Casimir interaction energy in a two-conductor waveguide for an arbitrary cross section. The idea is to combine a well-known method for computing eigenvalues of the Helmholtz equation, the point-matching technique [27], with the argument theorem to compute explicitly the sum over eigenfrequencies. Our technique is first tested for geometries with known solutions and then is applied to new geometries. Thus, in Sec. II we will describe the new approach. In Sec. III we validate our method against numerical results [10,21] obtained by us in previous works. In

*lombardo@df.uba.ar
†fmazzi@df.uba.ar
‡mariano.vazquez@bsc.es
§paula@df.uba.ar

the rest of the paper, we use our numerical approach to compute the Casimir interaction energy for more general cross sections of the waveguide, as corrugated cylinders in Sec. IV. In Sec. V A and V B we explore the behavior of the Casimir interaction energy between outer conductors that have focal lines and a cylindrical inner conductor. Concretely, Sec. V A shows the Casimir interaction energy when a cylinder with circular section is placed inside an outer cylinder with elliptical section. In Sec. V B, the outer conductor is a waveguide with parabolic section. Finally, in Sec. VI we expose our final remarks.

II. POINT-MATCHING NUMERICAL APPROACH

A two-conductor waveguide presents an interesting setup for the application of the point-matching technique. This technique has been widely used to solve eigenvalue problems in many areas of engineering science [27]. The boundary conditions are imposed at a finite number of points around the periphery of both conductors. Under this assumption, and for a solution proportional to $e^{-i\omega t}$, the partial differential equation of the problem can be reduced to a system of linear algebraic equations. The determinant associated to this system vanishes for some values of ω, the eigenfrequencies of the system, that can be determined in this way by searching the zeros numerically. In order to obtain the Casimir energy, instead of computing each eigenvalue, it is more convenient to use the argument theorem to perform the sum over all eigenvalues.

Let us consider a general geometry with translational invariance along the z axis (as, for example, very long and parallel conducting shells of arbitrary sections). We will bear in mind the situation in which one conductor encloses the other, as shown in Fig. 1, although the method could be applied to more general cases. The Casimir interaction energy for a system like this, composed of two conducting shells, can be written as

$$E_{12} = \frac{1}{2}\sum_p (w_p - \tilde{w}_p), \tag{1}$$

where w_p are the eigenfrequencies of the electromagnetic field satisfying perfect conductor boundary conditions on the surfaces of the conductors, and $\tilde{w}_p$ are those corresponding to a situation in which the external conducting shell is very large. Throughout this paper we use units $\hbar = c = 1$. The subindex p denotes the set of quantum numbers associated to each eigenfrequency. Introducing a cutoff for high frequency modes $E_{12}(\sigma) = \frac{1}{2}\sum_p (e^{-\sigma w_p} w_p - e^{-\sigma \tilde{w}_p}\tilde{w}_p)$, the Casimir interaction energy E_{12} is the limit of $E_{12}(\sigma)$ as $\sigma \to 0$. For simplicity we choose an exponential cutoff, although the explicit form is not relevant.

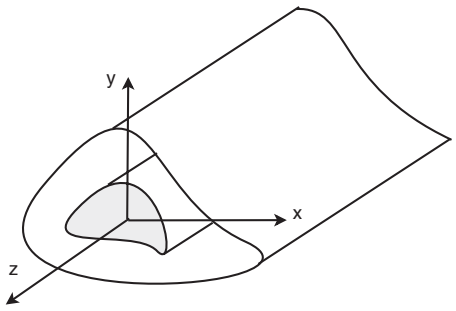

FIG. 1. A two-conductor waveguide in which one conductor encloses the other and each has an arbitrary cross section.

The transverse electric (TE) and transverse magnetic (TM) modes can be described in terms of two scalar fields, with adequate boundary conditions. In cylindrical coordinates, the modes of each scalar field will be of the form $h_{n,k_z}(t, r, \theta, z) = e^{(-iw_{n,k_z}t + ik_z z)}R_n(r, \theta)$, where the eigenfrequencies are $w_{n,k_z} = \sqrt{k_z^2 + \lambda_n^2}$, and λ_n are the eigenvalues of the two dimensional Laplacian

$$\left(\frac{\partial^2}{\partial r^2} + \frac{1}{r}\frac{\partial}{\partial r} + \frac{1}{r^2}\frac{\partial^2}{\partial \theta^2} + \lambda_n^2\right)R_n(r, \theta) = 0. \tag{2}$$

The set of quantum numbers p is given by (n, k_z). For very long cylinders of length L we can replace the sum over k_z by an integral. The result is

$$E_{12}(\sigma) = \frac{L}{2}\int_{-\infty}^{\infty}\frac{dk_z}{2\pi}\sum_n (\sqrt{k_z^2 + \lambda_n^2}e^{-\sigma\sqrt{k_z^2+\lambda_n^2}} - \sqrt{k_z^2 + \tilde{\lambda}_n^2}e^{-\sigma\sqrt{k_z^2+\tilde{\lambda}_n^2}}). \tag{3}$$

From the argument theorem it follows that

$$\frac{1}{2\pi i}\int_C d\lambda \lambda e^{-\sigma\lambda}\frac{d}{d\lambda}\ln f(\lambda) = \sum_i \lambda_i e^{-\sigma\lambda_i}, \tag{4}$$

where $f(\lambda)$ is an analytic function in the complex λ plane within the closed contour C, with simple zeros at $\lambda_1, \lambda_2, \ldots$ within C. We use this result to replace the sum over n in Eq. (3) by a contour integral

$$E_{12}(\sigma) = \frac{L}{4\pi i}\int_{-\infty}^{\infty}\frac{dk_z}{2\pi}\int_C d\lambda\sqrt{k_z^2 + \lambda^2}e^{-\sigma\sqrt{k_z^2+\lambda^2}}\frac{d}{d\lambda} \times \ln Q(\lambda). \tag{5}$$

Here the function $Q(\lambda)$ is the ratio $Q(\lambda) = F(\lambda)/\tilde{F}(\lambda)$ such that $F(\lambda)$ vanishes at λ_n and $\tilde{F}(\lambda)$ vanishes at $\tilde{\lambda}_n$ for all n.

To proceed we must choose an adequate contour for the integration in the complex plane (see [10] for details). We find

$$E_{12} = -\frac{L}{2\pi}\int_{-\infty}^{\infty}\frac{dk_z}{2\pi}\,\mathrm{Im}\left\{\int_0^{\infty} dy\sqrt{k_z^2 - y^2}\frac{d}{dy}\ln Q(iy)\right\}. \tag{6}$$

As we will see, $Q(iy)$ is a real function hence, the integral over y in Eq. (6) is restricted to $y > k_z$. After some straightforward steps one can rewrite this equation as

$$E_{12} = \frac{L}{4\pi}\int_0^\infty dy\, y \ln Q(iy). \tag{7}$$

As we have already mentioned, this expression is valid for conductors of arbitrary shape, as long as there is translational invariance along the z axis. The role of the point-matching method will be to provide an explicit expression for the function Q.

A general solution of the scalar Helmholtz equation (2) can be written as

$$R(r,\theta) = \sum_{m=-\infty}^{\infty} [A_m J_m(\lambda r) + B_m H_m^{(1)}(\lambda r)] e^{im\theta}, \tag{8}$$

where (r, θ) are the polar coordinates, and J_m and $H_m^{(1)}$ are the m-th order Bessel functions. The constants A_m and B_m are determined by the boundary conditions. For TM modes, the function R must verify Dirichlet boundary conditions on each conductor C_1 and C_2 (for TE modes, one should impose Neumann boundary conditions). The key point is to impose the boundary conditions on a finite number of points, as it is esquematically shown in Fig. 2. Therefore, for TM modes we have

$$0 = \sum_{m=-S}^{S} [A_m J_m(\lambda r_p) + B_m H_m^{(1)}(\lambda r_p)] e^{im\theta_p}, \tag{9}$$

$$0 = \sum_{m=-S}^{S} [A_m J_m(\lambda r_q) + B_m H_m^{(1)}(\lambda r_q)] e^{im\theta_q}, \tag{10}$$

where (r_p, θ_p) are points of the curve C_1 and (r_q, θ_q) belong to the curve C_2. We assume that with a finite number of terms, say $2S + 1$, we can acquire a desired computational accuracy in the solution. Thus, we should satisfy Eq. (9) and (10) at $2S + 1$ points on C_1 and C_2.

After imposing boundary conditions, we can write, in matrix form, the set of linear equations for the coefficients A_m and B_m in Eqs. (9) and (10)

$$M_1 A + M_2 B = 0, \qquad N_1 A + N_2 B = 0, \tag{11}$$

where $(M_1)_{pm} = J_m(\lambda r_p) e^{im\theta_p}$, $(M_2)_{pm} = H_m^{(1)}(\lambda r_p) e^{im\theta_p}$, $(N_1)_{qm} = J_m(\lambda r_q) e^{im\theta_q}$, and $(N_2)_{qm} = H_m^{(1)}(\lambda r_q) e^{im\theta_q}$. For this system to have nontrivial solutions, we shall ask that the determinant be zero. Thus, assuming that all matrices are square (i.e. there are $2S + 1$ points on each curve),

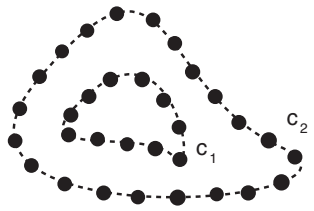

FIG. 2. Sections of the waveguides, indicating the points where we impose boundary conditions on each conductor.

$$\det\begin{bmatrix} M_1 & M_2 \\ N_1 & N_2 \end{bmatrix} = \det N_2 \cdot \det(M_1 - M_2 N_2^{-1} N_1) = 0. \tag{12}$$

This equation determines the eigenfrequencies associated to the geometry, and the usual approach in classical electromagnetism would be to find numerically its roots. However, as already mentioned, in order to compute the Casimir energy it is not necessary to find each eigenvalue. It is far more efficient to use the argument theorem, and obtain the sum over all eigenvalues as an integral in the complex plane. As this is in general a divergent quantity, we will compute the interaction zero-point energy by substracting the energy of the same geometric configuration but with a very large outer conductor. This means that we will have another set of equations similar to Eqs. (11) but evaluated on a different outer surface C_2^∞ (in which r_q is replaced by αr_q, with $\alpha \gg 1$)

$$\det\begin{bmatrix} M_1 & M_2 \\ N_1^\infty & N_2^\infty \end{bmatrix} \approx \det\begin{bmatrix} M_1 & M_2 \\ N_1^\infty & 0 \end{bmatrix} = \det[M_2 N_1^\infty] = 0. \tag{13}$$

In the equation above we have taken into account that, when using the argument theorem, all matrices will be evaluated on the imaginary axis. In this case, the different matrices become proportional to the modified Bessel functions

$$J_m(iyr_p) = i^m I_m(yr_p), \qquad H_m^{(1)}(iyr_p) = \frac{2}{\pi}(-i)^m K_m(yr_p). \tag{14}$$

After these substitutions, it is easy to check that the matrix N_2^∞ vanishes in the limit $\alpha \to \infty$. Then, in order to compute the finite interaction energy with the argument theorem, the relevant determinant is

$$\det[(M_1 - M_2 N_2^{-1} N_1) M_2^{-1} (N_1^\infty)^{-1}]. \tag{15}$$

Neglecting the self-energies of each configuration (that do not contribute to the interaction energy between the conductors), we obtain the expression for the function Q to be included in the expression for the Casimir interaction energy in Eq. (7):

$$\begin{aligned} Q(iy) &= \det[I - M_1 N_1^{-1} N_2 M_2^{-1}] \\ &= \det[I - \tilde{M}_1 \tilde{N}_1^{-1} \tilde{N}_2 \tilde{M}_2^{-1}], \end{aligned} \tag{16}$$

where

$$\begin{aligned} (\tilde{M}_1)_{pm} &= I_m(yr_p) e^{im\theta_p}, & (\tilde{M}_2)_{pm} &= K_m(yr_p) e^{im\theta_p}, \\ (\tilde{N}_1)_{qm} &= I_m(yr_q) e^{im\theta_q}, & (\tilde{N}_2)_{qm} &= K_m(yr_q) e^{im\theta_q}. \end{aligned} \tag{17}$$

Note that the factors that multiply the modified Bessel functions in Eq. (14) cancel out in the function Q.

There are similar expressions for the TE modes, in which each Bessel function is replaced by its derivative. The full Casimir interaction energy is given by the sum of the TE and TM contributions.

As a first example, we consider the case of having a configuration of concentric cylinders. In that case, the points on curve C_1 are all on a circle of radii $r_p = a$, i.e. we are choosing points of coordinate (a, θ_p). Similarly, points on the outer cylinder of radii b will be (b, θ_q) since we can choose points with the same polar angle θ_p but of different radial distance. In such a case, the matrices can be factorized as

$$(\tilde{M}_1)_{pm} = \Theta_{pm} I_m(ya), \qquad (\tilde{M}_2)_{pm} = \Theta_{pm} K_m(ya),$$
$$(\tilde{N}_1)_{pm} = \Theta_{pm} I_m(yb), \qquad (\tilde{N}_2)_{pm} = \Theta_{pm} K_m(yb). \tag{18}$$

Here Θ is the matrix that contains the angular contribution

$$\Theta_{pm} = \exp\{im\theta_p\}, \tag{19}$$

where, in the case of circular sections, we have $\theta_p = 2\pi p/(2S+1)$. Inserting Eqs. (18) and (19) into Eq. (16) we find

$$Q(iy) = \det\left[1 - \frac{I(ya)K(yb)}{I(yb)K(ya)}\right], \tag{20}$$

where we introduced diagonal matrices I and K. In this way, we reobtain the known expression for the TM Casimir energy for concentric cylinders [8]:

$$E_{12}^{cc,TM} = \frac{L}{4\pi}\int_0^\infty dy y \ln\left(\prod_m \left[1 - \frac{I_m(ya)K_m(yb)}{I_m(yb)K_m(ya)}\right]\right)$$

For the TE modes the Casimir energy is given by a similar expression, in which each Bessel function is replaced by its derivative.

We have developed a numerical Fortran routine in order to evaluate the Casimir interaction energy for a two-conductor waveguide of arbitrary cross sections. With a two dimensional mesh and the use of $2S+1$ points on each curve, we define the cross section of the waveguide. Once the points are selected, we impose Dirichlet and Neumann boundary conditions on each of them and define the $\tilde{M}$'s and $\tilde{N}$'s matrices. Then we use a standard Fortran routine to invert the matrices and define the matrix whose determinant gives the Q function [see Eq. (16)] to be included in Eq. (7). Finally, we calculate the determinant and perform an integration over all values of y. The parameters used by the program are: the number of points used to define the geometry $2S+1$, the integration limit ($y_{\max}$), and the precision desired.

Since in the final expression for the interaction energy the ultraviolet divergences have been removed, the main contribution comes from modes whose wavelengths do not fall much below the characteristic distances of the configuration (geometric sizes of the interacting bodies, minimun distance between them). For this reason we expect that the energy can be computed accurately if enough points are taken, as in the case of the scattering approach to Casimir forces [28].

The number of points on the surfaces rules the bigger order of the Bessel functions involved in our simulations, and this means that, sometimes, special precautions have to be taken to maintain accuracy of computation (such as the approximation for small argument for the modified Bessel functions). However, we should remark that, though its limitation in the number of points selected, this technique is of great use for evaluating the TE and TM contributions to the energy. In the case of smooth geometries, we shall see that the number of points selected is enough to reproduce results in excellent agreement with previous calculations.

Finally, we would like to mention that the choice of the functions used to described the general solution to the Helmholtz equation (Bessel and complex exponential functions in our case) depends on the cross section of the waveguide. Other geometries could also be worked out using a different set of complete functions.

III. TESTING THE METHOD: ECCENTRIC CYLINDERS

We shall begin by applying the point-matching approach to the case of two eccentric cylinders. In this case, we can check our simulations against our previous numerical work [21]. Therein, we numerically evaluated the Casimir interaction energy for two eccentric cylinders using the formula

$$E_{12} = \frac{L}{4\pi}\int_0^\infty dy y[\ln(M^{\mathrm{TE}}(y)) + \ln(M^{\mathrm{TM}}(y))],$$

where $M^{\mathrm{TM}}(y) = \det[\delta_{np} - A_{n,p}^{\mathrm{TM}}]$ and $M^{\mathrm{TE}}(y) = \det[\delta_{np} - A_{n,p}^{\mathrm{TE}}]$. The matrices $A_{n,p}^{\mathrm{TM}}$ and $A_{n,p}^{\mathrm{TE}}$ were analytically derived in a previous work [10]. Herein, we shall evaluate the Casimir interaction energy by the use of the point-matching technique. We will follow the notation of Ref. [10], denoting by a and b the radii of the inner and outer cylinders, respectively, and by ϵ the eccentricity of the configuration (distance between the axes of the cylinders). The adimensional quantities $\delta = \epsilon/a$ and $\alpha = b/a$ will be useful to describe the numerical results.

The comparison between the new and old approaches for the evaluation of the Casimir interaction energy between eccentric cylinders was done for several runs with the same parameters in both programs. In this case we used a mesh of 21 points for simulating each cylinder, and matrices of 21×21 in our old approach. In this way, we are able to reobtain Figs. 2 and 3 of our previous work [21] as can be seen in Figs. 4 and 5, where we plot the interaction energy for eccentric cylinders for different values of the radii and the eccentricity, using both methods. It is easy to note in Figs. 4–6 that the difference among them is less than the

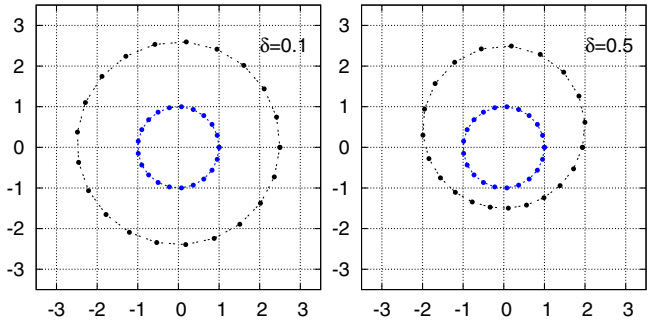

FIG. 3 (color online). Numerical mesh and points used in the point-matching method for simulating the boundaries between two eccentric cylinders. In this case, we show two different values of α and of the eccentricity δ. For simplicity, for each point on the inner cylinder we choose a point on the outer cylinder with the same angular coordinate.

2% in the case of $\alpha \geq 2$ and $\delta \leq 0.5$. The error can be blamed on the bigger quantity of algebraic operations contained in the new approach. It is worth mentioning that adding one more point to the point-matching method, i.e. having 23 points in each circle, represents a variation in our result of only 0.000 004% for $\alpha = 3$ and $\delta = 0.1$ and 0.0004% for $\alpha = 2$ and $\delta = 0.1$. Thus, we see the great agreement between both approaches. As can be seen from Figs. 6 and 7, small deviations appear for large eccentricities and small α. We expect the precision in these cases to be improved by considering grids with a larger number and/or a nonuniform distribution of points on the surfaces.

In Fig. 8 we show the comparison between the new and old approaches for concentric ($\delta = 0$) cylinders, as a func-

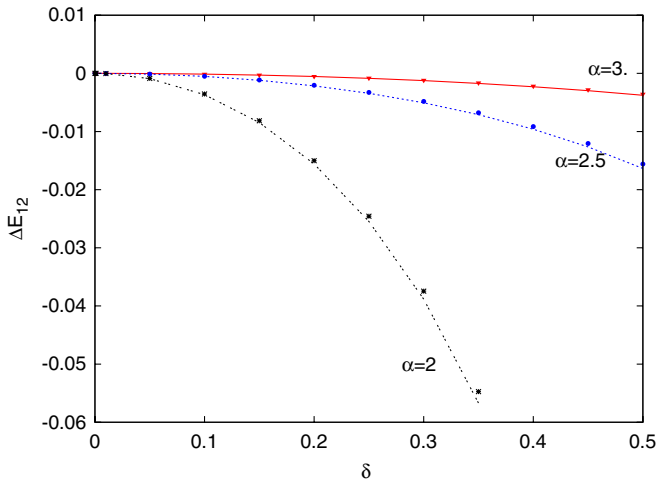

FIG. 4 (color online). Comparison between the point-matching method (set in the plot as new) and the numerical method used in Ref. [21] (set as old) for numerically evaluating the Casimir energy as a function of the eccentricity δ for different values of $\alpha = b/a$. ΔE_{12} refers to the energy difference between the eccentric and the concentric configurations. Energies are measured in units of $L/4\pi a^2$.

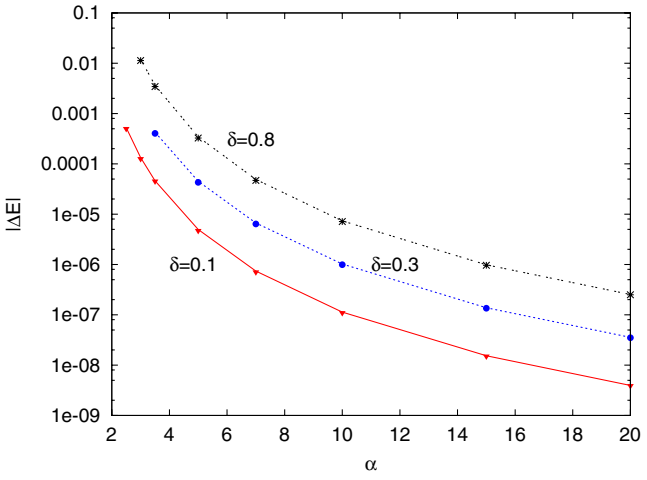

FIG. 5 (color online). Comparison between the new and old approaches for the evaluation of the Casimir energy differences as a function of $\alpha = b/a$ for different values of the eccentricity δ. Energies are measured in units of $L/4\pi a^2$.

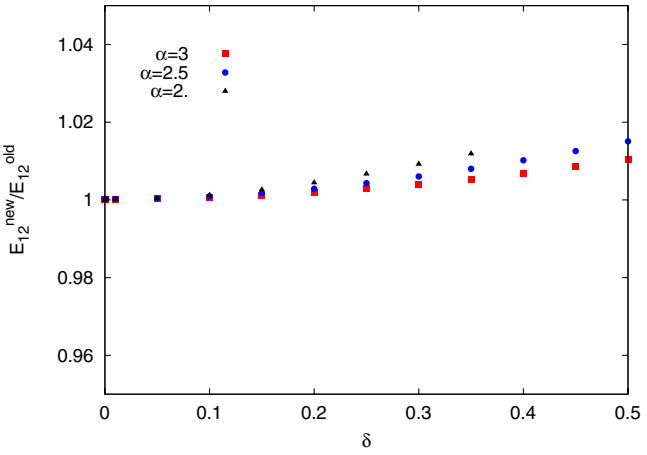

FIG. 6 (color online). Ratio between the Casimir energies evaluated using the new and the old approaches, as a function of the eccentricity δ for different values of $\alpha = b/a$.

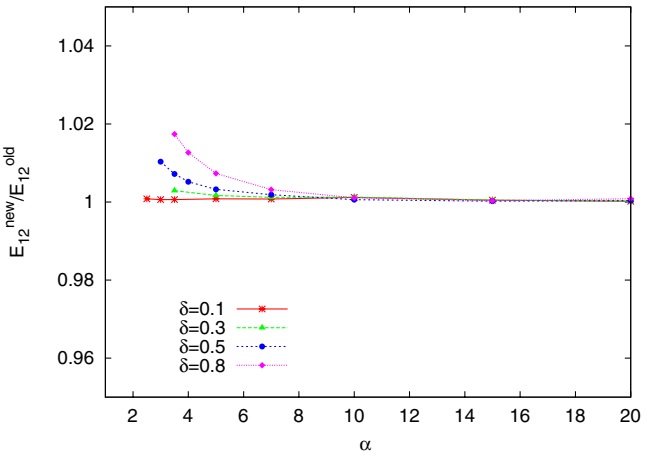

FIG. 7 (color online). Ratio between the Casimir energies evaluated using the new and the old approaches, as a function of $\alpha = b/a$ for three different values of δ. Energies are measured in units of $L/4\pi a^2$.

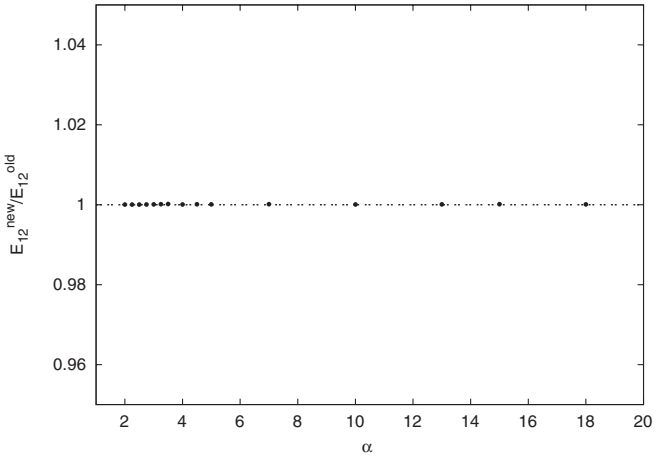

FIG. 8. Comparison between the new and old approach for numerically evaluating the Casimir interaction energy in the concentric case ($\delta = 0$), as a function of $\alpha = b/a$. The point-matching approach is greatly accurate in this case.

tion of α. In this case, the agreement between the full numerical and the point-matching approaches is even better.

IV. CYLINDRICAL RACK AND PINION

When two concentric cylinders have corrugations, the vacuum energy produces a torque that could, in principle, make one cylinder rotate with respect to the other. This "cylindrical rack and pinion" has been proposed in Ref. [29], where the torque has been computed using the proximity force approximation. It was further analyzed in [30], where the authors obtained perturbative results for Dirichlet boundary conditions in the limit of small amplitude corrugations. In this section, we numerically evaluate the Casimir interaction energy for two concentric corrugated cylinders. The cylinders have radii a and b, and we will denote by $r_- = b - a$ the mean distance between them and by $r_+ = a + b$ the sum of the radii. As in the previous section, we will use the notation $\alpha = b/a$. In Fig. 9 we show two geometries with different frequencies associated to the corrugations: on the left side, $\nu = 3$ and on the right side $\nu = 5$, both for $\alpha = 2$. The points in the mesh are described by the following functions:

$$h_a(\theta) = h\sin(\nu\theta), \qquad h_b(\theta) = h\sin(\nu\theta + \phi_0), \quad (21)$$

where h is the corrugation amplitude and ν is the frequency associated with these corrugations. The Casimir torque can be calculated by taking the derivative of the interaction energy with respect to the shifted angle $\mathcal{T} = -\partial E_{12}/\partial\phi_0$. In the case of the TM mode (Dirichlet boundary conditions), details of the perturbative calculation can be found in Ref. [30]. Therein, the authors obtained an analytical expression for the Casimir interaction energy as a function of the angle ϕ_0 for small h, which reads

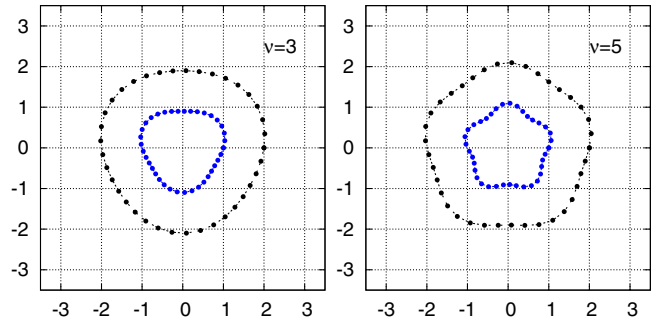

FIG. 9 (color online). Numerical mesh and points used in the point-matching method for simulating the boundaries between two concentric cylinders with harmonic corrugations. In this case, we show $\alpha = 2$, $\phi_0 = 0$, for two different values of ν.

$$\frac{E_{12}}{\pi r_+ L} = \cos(\nu\phi_0)\frac{\pi^2}{240 r_-^5} h^2 B_\nu^{(2)D}(y), \quad (22)$$

where $y = r_-/r_+$ and $B_\nu^{(2)D}(y)$ is given by

$$B_\nu^{(2)D}(y) = \frac{15}{\pi^4}\sum_{m=-\infty}^{+\infty} 8y^3 \int_0^\infty x\,dx \frac{4y^2}{(1-y^2)}\frac{1}{D_m(y,x)} \times \frac{1}{D_{m+\nu}(y,x)}. \quad (23)$$

The functions D_m are given by

$$D_m(y;x) = I_m(x[1+y])K_m(x[1-y]) - I_m(x[1-y])K_m(x[1+y]). \quad (24)$$

In Fig. 10 we show the numerical evaluation of the TM Casimir interaction energy for this geometry. The plot shows the results obtained using our point-matching ap-

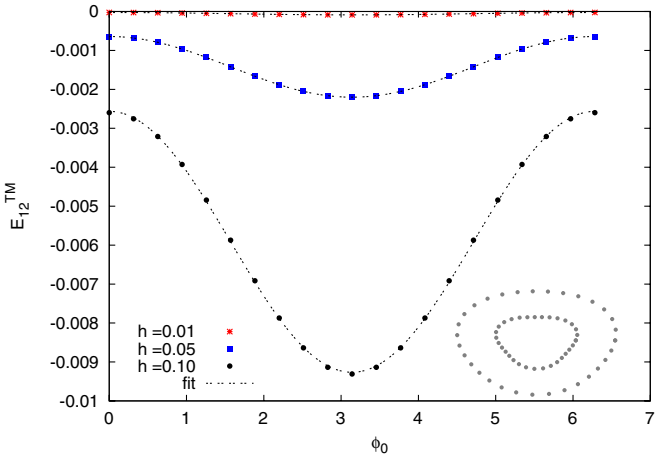

FIG. 10 (color online). Casimir interaction energy (TM modes) as a function of ϕ_0 for $\alpha = 2$ and different values of perturbation $\tilde{h} = h/a$. The different shaped dots are the numerical data obtained with our program while the line represents the numerical fit of each curve. Energies are measured in units of L/a^2.

proach with $\alpha = 2$ and corrugation frequency $\nu = 3$, for different values of the amplitude of the corrugation h. As expected the amplitude of the oscillations grows with h. For each value of h we have performed a numerical fit of the data in order to compare with the analytical prediction presented in Eq. (22). With dotted lines we have plotted the fit $y(x) = A * \cos(x)$ for each curve in Fig. 10. The agreement between dots and dotted lines is extremely good.

In Table I, we can see the comparison between the analytical prediction and our numerical results for different values of α, ν, and $\tilde{h} = h/a$. For each simulation we have used a mesh of 37–41 points, depending the value of $\tilde{h}$. For $\alpha = 2$ and $\tilde{h} = 0.1$, having 31 or 37 points selected to define each boundary has a relative error of 0.000 04% in the final value of the energy. For $\nu = 5$, this difference is approximately 0.002%, as one can anticipate (for a smoother curve less points are needed in order to achieve the same accuracy in the result). In the table, we can see that for small values of $\tilde{h}$, the values of the amplitude of the numerical fit of the data are extremely similar to those predicted analytically. However, we must note that this technique does not have a constraint on the value of $\tilde{h}$ so far. For bigger values of $\tilde{h}$ one has to include more points in the mesh so as to have a well-defined geometry and maintain accuracy in the results, that differ from the analytical predictions.

In addition, in Fig. 11 we have presented the evaluation of the Casimir interaction energy for the Neumann (TE) modes. Therein, we see that the behavior is qualitatively similar to that of the Dirichlet modes, with a different value for each numerical fit of the data points. It is worth emphasizing that there are no analytical predictions for this mode so far, being this the first evaluation of the TE Casimir interaction energy for corrugated concentric cylinders.

It is worth remarking that, when the amplitude of the corrugation is not very small, the exact results cannot be reproduced with a simple fit of the form $y(x) = A * \cos(x)$. This is illustrated in Fig. 12, where we see that, for the biggest corrugated amplitude that we included in Table I ($\tilde{h} = 0.3$), the exact result differs from the cosine function.

Finally, in Fig. 13 we show the different contributions of the TM and TE modes to the interaction energy for bigger values of α. As expected from previous results [10], for large values of α, the Dirichlet contribution is bigger (in absolute value) than the Neumann one.

TABLE I. Comparison between the analytical [Eq. (22)] and numerical predictions [fit of the form $y(x) = A * \cos(x)$] of the Casimir interaction energy (Dirichlet modes) for different configurations of the concentric corrugated cylinders.

ν	α	$\tilde{h}$	A (Analytical)	A (Numerical)
3	2	0.01	0.000 030 414	0.000 030 44
3	2	0.05	0.000 760	0.000 77
3	2	0.1	0.0030	0.0033
3	2	0.3	0.027	0.078
3	3.5	0.01	0.000 003 925	0.000 003 928
3	3.5	0.05	0.000 098 1	0.000 099 3
3	3.5	0.1	0.000 392	0.000 412
3	3.5	0.3	0.003 53	0.005 67
5	2	0.01	0.000 020 46	0.000 020 49
5	2	0.05	0.000 511	0.000 528
5	2	0.1	0.002 04	0.002 32
5	2	0.3	0.018	0.071

V. OUTER CONDUCTORS WITH FOCAL LINES

Some time ago, there was a conjecture [31] based on a geometric optics approximation, about the possibility of focusing vacuum fluctuations in parabolic mirrors. It was argued that a parabolic mirror is capable of focusing the vacuum modes of the quantized electromagnetic field, therefore creating large physical effects near the mirror's focus. The physical manifestation of this focusing is a growth in the energy density and mean-squared electric field as the focus is approached. In particular, the energy density would diverge as the inverse fourth power of the distance from the focus in the case of perfect conductivity. These results would imply that the focused vacuum fluctuations will enhance Casimir forces on atoms or other particles near the focus. The sign of the force could draw particles into the vicinity of the focus [31].

With this motivation, in this section we shall evaluate the Casimir interaction energy for configurations in which the outer conducting shell has a cross section that contains focal points.

A. Cylinder inside an ellipse

To begin with, we will compute the Casimir interaction energy between one small inner cylinder and an outer

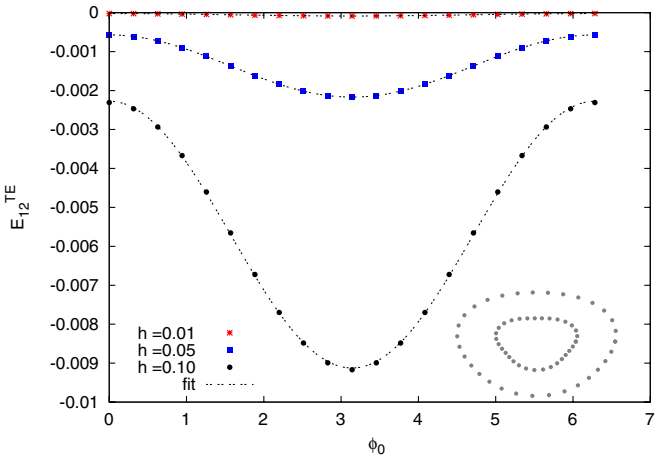

FIG. 11 (color online). Casimir interaction energy (TE modes) as a function of ϕ_0 for a value $\alpha = 2$ and different values of perturbation $\tilde{h}$. The different shaped dots are the numerical data obtained with our program while the line represents the numerical fit of each curve. Energies are measured in units of L/a^2.

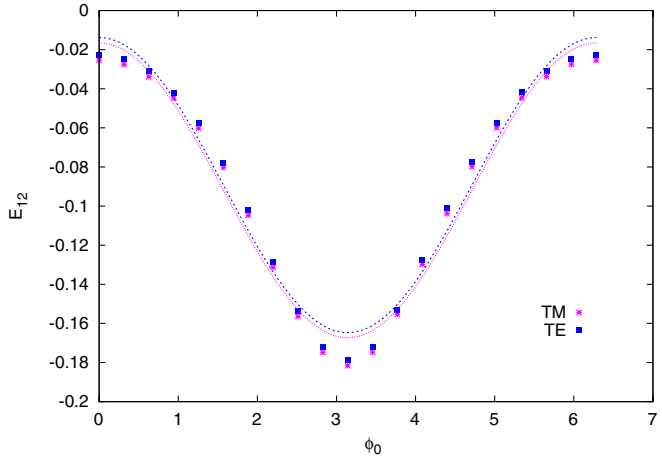

FIG. 12 (color online). Casimir interaction energy (TE and TM modes) as a function of ϕ_0 for $\alpha = 2$, $\nu = 3$, and $\tilde{h} = 0.3$. The different shaped dots are the numerical data obtained by our program while the line represents the numerical fit of each curve. In this case, the plot shows that the exact result cannot be fitted by a function $y(x) = A * \cos(x)$. Energies are measured in units of L/a^2.

ellipse, by the use of the point-matching method. We will denote by a the radius of the inner cylinder, by b_1 and b_2 the minor and major semiaxes of the ellipse, respectively, and by f the distance between the foci and the center of the ellipse. The coordinates of the center of the cylinder with respect to the center of the ellipse will be (ϵ_x, ϵ_y). We will use an additional tilde to denote adimensional quantities, i.e distances in units of a: $\tilde{b}_i = b_i/a$, $\tilde{f} = f/a$, etc.

For this configuration, we use a mesh like the one presented in Fig. 14, where we show an inner cylinder, and an outer ellipse with semiaxes $\tilde{b}_1 = 4$ and $\tilde{b}_2 = 4.33$.

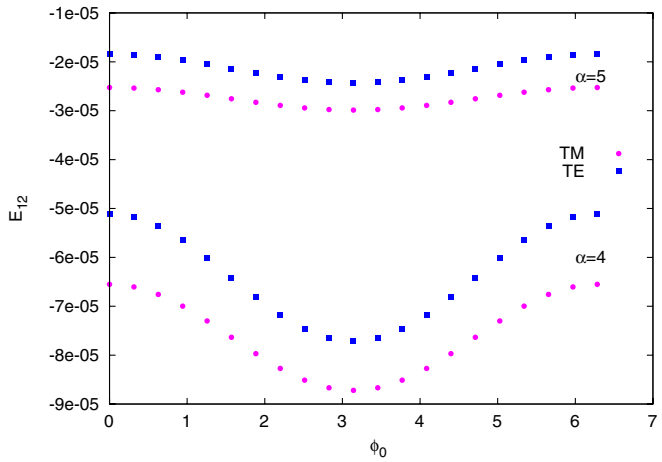

FIG. 13 (color online). TM and TE contributions to the Casimir interaction energy in the concentric corrugated case. The Dirichlet (TM) contribution is bigger than the Neumann (TE) one (in absolute value).

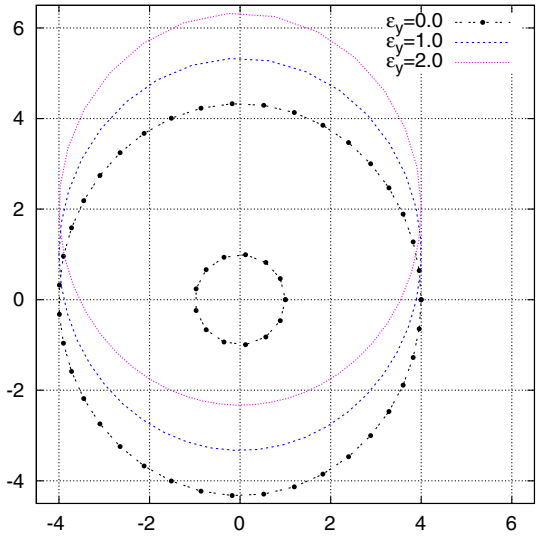

FIG. 14 (color online). Mesh used to evaluate the boundary conditions in the framework of the point-matching method. We represent a small centered cylinder and vary the position of the outer ellipse. Parameters used: minor ellipse semiaxis $\tilde{b}_1 = 4$, major ellipse semiaxis $\tilde{b}_2 = 4.33$, and focal position $\tilde{f} = 1.66$.

The ellipse has two focal points at $\tilde{f} = 1.66$. We present the results for the Casimir energy in Figs. 15 and 16.

From Fig. 15 it is possible to see that there is an unstable equilibrium position at the origin under displacements of the inner cylinder along the (vertical) ϵ_y direction. As expected, it is also possible to check that the energy grows as well as the cylinder gets closer to the surface of the outer ellipse. Figure 15 also shows a monotonic behavior of the energy as a function of the position, even when passing through the focus. Otherwise, Fig. 16 shows the unstable equilibrium position at the origin when moving the inner cylinder in the (horizontal) ϵ_x direction. It is also important

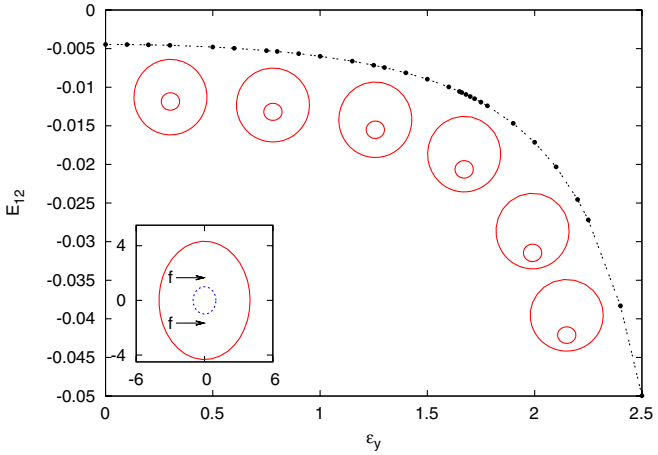

FIG. 15 (color online). Numerical evaluation of the Casimir interaction energy for an inner cylinder an eccentric outer ellipse, as a function of the position of the cylinder along the vertical axis. Energies are measured in units of L/a^2.

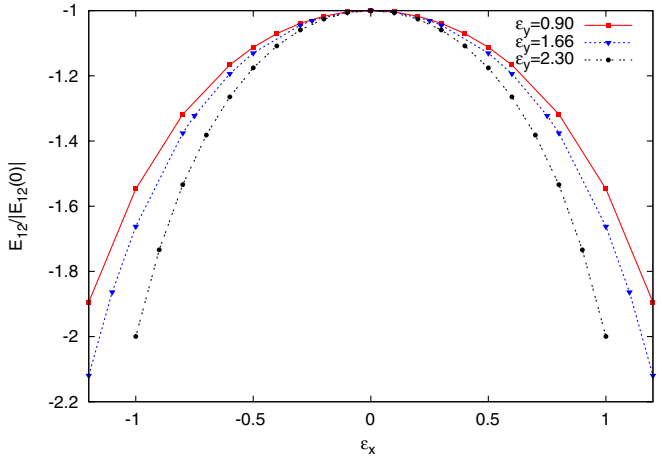

FIG. 16 (color online). Moving the inner cylinder along the minor semiaxis the ellipse we show that the center of the ellipse is an unstable equilibrium position. This is shown for different positions of the inner cylinder along the major semiaxis. Energies are normalized to the value of $|E_{12}(\epsilon_x = 0)|$.

to stress that, when considering horizontal displacements at a fixed vertical position, the higher the altitude of the inner cylinder, the narrow the inverted potential in Fig. 16.

B. Cylinder inside a Parabola

Following the same idea than in the previous subsection, here we describe the numerical computation of the Casimir interaction energy for a small inner cylinder with circular cross section, inside a large cylinder with parabolic section. In Fig. 17 we show the two dimensional cross section of the mesh used to simulate this geometry and impose the boundary conditions. The parameters for this case are the

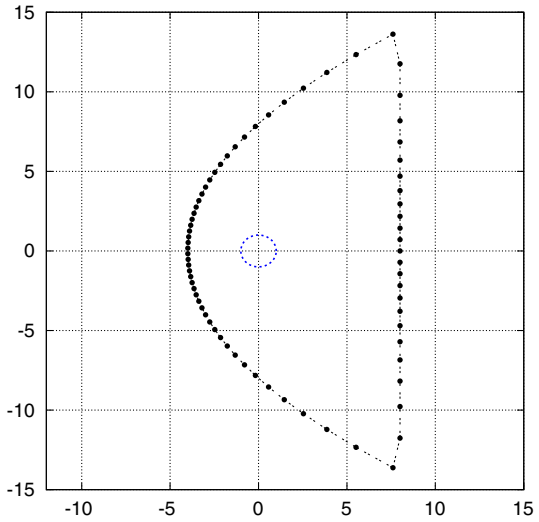

FIG. 17 (color online). Mesh used to evaluate the boundaries condition in the framework of the point-matching method. We represent a small centered cylinder and vary the value of the position of the outer parabola. Parameter used $\tilde{f} = 4$.

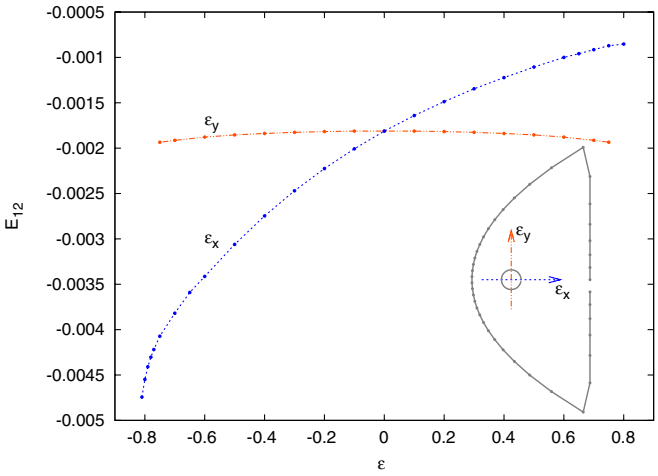

FIG. 18 (color online). Numerical evaluation of the Casimir interaction energy between an inner cylinder inside a bigger parabola. We move the inner cylinder both in directions ϵ_x and ϵ_y. Parameter used: $\tilde{f} = 4$. Energies are measured in units of L/a^2.

radius of the inner cylinder, a, and the focal distance of the parabola, f. As before, we introduce $\tilde{f} = f/a$.

In Fig. 18, we show the behavior of the Casimir interaction energy with the position of the inner cylinder. The number of points used is approximately 40. It is easy to see that the bigger increase of the energy (and therefore of the force) is in the direction labeled as ϵ_x. We can also note an increase in the energy as the inner cylinder gets closer to the vertex of the parabola (in the ϵ_x direction), a by-product of the proximity between the inner cylinder surface and the one corresponding to the parabola. On the other hand, as the behavior of the energy is symmetric in the ϵ_y direction, the force F_y vanishes on the horizontal axis. There is also an unstable equilibrium position at a particular point on this axis, as it is suggested by Fig. 18.

As in the previous example, the energy and the force do not have a special behavior near the focus. It would be interesting to check if this behavior is a general feature, i.e if it is independent of the size of the inner cylinder and/or the shape of the outer conductor. To analyze this problem in more detail, it is necessary to consider a much larger number of points on the surfaces, since the distance between nearest neighbor dots should be smaller than the minimum length scale of the geometry. To address this issue it is mandatory to improve the computational procedure, in order to handle numerically Bessel functions of very large order.

VI. FINAL REMARKS

In this paper we presented a new numerical method to compute the vacuum energy for arbitrary geometries with translational invariance. The method is based on the use of the point-matching approach, in which the boundary con-

ditions are imposed on a discrete set of points on the surfaces of the conducting bodies. This approach is combined with the argument theorem, in order to trade the sum over eigenvalues for an integral in the complex plane.

After testing our method against previous results, we have computed the Casimir interaction energy for new geometries. In the case of the cylindrical rack and pinion described in Sec. IV, we have seen that, for corrugations of small amplitude, the numerical results for the energy show a harmonic dependence with the shifted angle, and a quadratic dependence with the amplitude of corrugations, in agreement with previous analytic perturbative evaluations. This behavior disappears for larger amplitudes, where the exact results show more pronounced peaks.

In Sec. V we computed the Casimir interaction energy between an inner cylinder and outer surfaces with focal lines. The motivation for looking at these configurations was to see whether there was a non trivial behavior of the energy near the focus or not. For both cases considered (ellipses and parabolas), we have found that the energy and forces are monotonic across the focal lines. This may be a peculiarity of the geometries with translational invariance considered here. We have also confirmed the existence of unstable equilibrium positions of the inner cylinder, that coincide with the location suggested by simple geometric arguments.

The examples discussed in this paper illustrate the simplicity and power of this approach. We have used a straightforward version of the point-matching method, with a naive choice of the points on the curves (note that in all examples we have chosen pair of points with the same angular coordinate with respect to the inner cylinder). For less symmetric configurations, and when the surfaces of both conductors are closer to each other, it will be necessary to consider grids with a larger number of points, and to optimize their positions. As in the applications to acoustic or classical electromagnetism, special care must be taken for surfaces with pronounced edges, clefts, or ''handles,'' where the point-matching technique may not be accurate to determine the eigenfrequencies.

It is certainly possible to go beyond the geometries considered here. Still considering geometries with translation invariance along the z axis, it would be possible to analyze waveguides with more than two conducting bodies. The generalization for nonperfect mirrors is also possible. For the case of scalar fields satisfying arbitrary matching conditions on the surfaces (rather than Dirichlet or Neumann boundary conditions), the generalization is relatively straightforward. However, for the electromagnetic field the calculation is more cumbersome, since in general it will be not possible to treat independently the TE and TM modes.

The point-matching approach can also be generalized to three dimensional compact objects. The starting point in this case would be the solutions of the three dimensional Helmholtz equation, written in terms of an adequate basis (products of spherical Bessel functions and spherical harmonics). We expect these geometries to require much more computational effort, and a more sophisticated method to optimize the choice of the grid of points on which the boundary conditions are imposed.

ACKNOWLEDGMENTS

This work has been supported by CONICET, UBA, and ANPCyT, Argentina. P. I. V. would like to thank the hospitality of the Barcelona Supercomputing center, where part of this work was done.

[1] H. B. G. Casimir, Proc. K. Ned. Akad. Wet. **51**, 793 (1948); For recent reviews see M. Bordag, U. Mohideen , and V. M. Mostepanenko, Phys. Rep. **353**, 1 (2001); K. A. Milton, *The Casimir Effect: Physical Manifestations of the Zero-Point Energy* (World Scientific, Singapore, 2001); S. Reynaud *et al.*, C. R. Acad. Sci. Ser. IV: Phys., Astrophys. **2**, 1287 (2001); K. A. Milton, J. Phys. A **37**, R209 (2004); S. K. Lamoreaux, Rep. Prog. Phys. **68**, 201 (2005); M. Bordag, G. L. Klimchitskaya, U. Mohideen, and V. M. Mostepanenko, *Advances in the Casimir Effect* (Oxford University Press, Oxford, 2009).

[2] G. Bressi, G. Carugno, and G. Ruoso, Phys. Rev. Lett. **88**, 041804 (2002).

[3] S. K. Lamoreaux, Phys. Rev. Lett. **78**, 5 (1997); U. Mohideen and A. Roy, Phys. Rev. Lett. **81**, 4549 (1998); B. W. Harris, F. Chen, and U. Mohideen, Phys. Rev. A **62**, 052109 (2000); H. B. Chan, V. A. Aksyuk, R. N. Kleiman, D. J. Bishop, and F. Capasso, Science **291**, 1941 (2001); Phys. Rev. Lett. **87**, 211801 (2001); D. Iannuzzi, I. Gelfand, M. Lisanti, and F. Capasso, Proc. Natl. Acad. Sci. U.S.A. **101**, 4019 (2004); D. E. Krause, R. S. Decca, D. Lopez, and E. Fischbach, Phys. Rev. Lett. **98**, 050403 (2007); R. S. Decca, D. Lopez, E. Fischbach, G. L. Klimchitskaya, D. E. Krause, and V. M. Mostepanenko, Phys. Rev. D **75**, 077101 (2007); F. Chen, G. L. Klimchitskaya, V. M. Mostepanenko, and U. Mohideen, Phys. Rev. B **76**, 035338 (2007); H. B. Chan *et al.*, Phys. Rev. Lett. **101**, 030401 (2008).

[4] T. Ederth, Phys. Rev. A **62**, 062104 (2000).

[5] M. Brown-Hayes, D. A. R. Dalvit, F. D. Mazzitelli, W. J. Kim, and R. Onofrio, Phys. Rev. A **72**, 052102 (2005).

[6] R. Ardito *et al.*, IEEE Sensors 2008 Conference p. 90 (2008).

[7] A. A. Saharian, ICTP Report No. IC/2000/14.

[8] F. D. Mazzitelli, M. J. Sánchez, N. N. Scoccola, and J. von Stecher, Phys. Rev. A **67**, 013807 (2003).

[9] D. A. R. Dalvit, F. C. Lombardo, F. D. Mazzitelli, and R. Onofrio, Phys. Rev. A **74**, 020101 (2006).
[10] F. D. Mazzitelli, D. A. R. Dalvit, and F. C. Lombardo, New J. Phys. **8**, 240 (2006).
[11] M. Schaden and L. Spruch, Phys. Rev. A **58**, 935 (1998); Phys. Rev. Lett. **84**, 459 (2000).
[12] R. Golestanian and M. Kardar, Phys. Rev. A **58**, 1713 (1998); T. Emig, A. Hanke, and M. Kardar, Phys. Rev. Lett. **87**, 260402 (2001); T. Emig and R. Buscher, Nucl. Phys. **B696**, 468 (2004); T. Emig, R. L. Jaffe, M. Kardar, and A. Scardicchio, Phys. Rev. Lett. **96**, 080403 (2006); M. Bordag, Phys. Rev. D **73**, 125018 (2006).
[13] A. Bulgac, P. Magierski, and A. Wirzba, Phys. Rev. D **73**, 025007 (2006); A. Wirzba, A. Bulgac, and P. Magierski, J. Phys. A **39**, 6815 (2006).
[14] R. Balian and B. Duplantier, Ann. Phys. (N.Y.) **112**, 165 (1978); **104**, 300 (1977).
[15] K. Milton and J. Wagner, J. Phys. A **41**, 155402 (2008).
[16] H. Gies, K. Langfeld, and L. Moyaerts, J. High Energy Phys. 06 (2003) 018.
[17] A. Rodriguez, M. Ibanescu, D. Iannuzzi, F. Capasso, J. D. Joannopoulos, and S. G. Johnson, Phys. Rev. Lett. **99**, 080401 (2007).
[18] T. Emig, R. J. Jaffe, M. Kardar, and A. Scardicchio, Phys. Rev. Lett. **96**, 080403 (2006); M. Bordag, Phys. Rev. D **73**, 125018 (2006).
[19] T. Emig, J. Stat. Mech. (2008) P04007.
[20] P. A. Maia Neto, A. Lambrecht, and S. Reynaud, Phys. Rev. A **78**, 012115 (2008).
[21] F. C. Lombardo, F. D. Mazzitelli, and P. I. Villar, Phys. Rev. D **78**, 085009 (2008).
[22] T. Emig, N. Graham, R. L. Jaffe, and M. Kardar, Phys. Rev. Lett. **99**, 170403 (2007).
[23] T. Emig, A. Hanke, R. Golestanian, and M. Kardar, Phys. Rev. Lett. **87**, 260402 (2001); A. Lambrecht and V. N. Marachevsky, Int. J. Mod. Phys. A **24**, 1789 (2009).
[24] R. M. Cavalcanti, Phys. Rev. D **69**, 065015 (2004); M. P. Hertzberg, R. L. Jaffe, M. Kardar, and A. Scardicchio, Phys. Rev. D **76**, 045016 (2007); V. N. Marachevsky, Phys. Rev. D **75**, 085019 (2007); S. A. Fulling and J. H. Wilson, Phys. Rev. A **76**, 012118 (2007); A. Edery, Phys. Rev. D **75**, 105012 (2007); X. Zhai and X. Li, Phys. Rev. D **76**, 047704 (2007); V. N. Marachevsky, J. Phys. A **41**, 164007 (2008); K. Kirsten and S. A. Fulling, Phys. Rev. D **79**, 065019 (2009); A. Edery and V. Marachevsky, Phys. Rev. D **78**, 025021 (2008); K. Kirsten and S. A. Fulling, Phys. Rev. D **79**, 065019 (2009); L. P. Teo, J. Phys. A **42**, 105403 (2009); E. Alvarez and F. D. Mazzitelli, Phys. Rev. D **79**, 045019 (2009).
[25] S. J. Rahi, A. W. Rodriguez, T. Emig, R. L. Jaffe, S. G. Johnson, and M. Kardar, Phys. Rev. A **77**, 030101(R) (2008); S. J. Rahi, T. Emig, R. L. Jaffe, and M. Kardar, Phys. Rev. A **78**, 012104 (2008); M. Bordag and V. Nikolaev, arXiv:0904.0664.
[26] T. Emig, N. Graham, R. L. Jaffe, and M. Kardar, Phys. Rev. A **79**, 054901 (2009).
[27] R. Bates, IEEE Trans. Microwave Theory Tech. **MTT-17**, 297 (1969); H. Y. Yee and N. F. Audeh, IEEE Trans. Microwave Theory Tech. **13**, 847 (1965); **14**, 487 (1966); J. R. Kuttler and V. G. Sigillito, SIAM Rev. **26**, 163 (1984) and references therein. For a generalization and applications to scattering problems see F. M. Kahnert, J. Quant. Spectrosc. Radiat. Transfer **79–80**, 775 (2003) and references therein.
[28] O. Kenneth and I. Klich, Phys. Rev. B **78**, 014103 (2008); Phys. Rev. Lett. **97**, 160401 (2006).
[29] F. D. Mazzitelli, F. C. Lombardo, and P. I. Villar, J. Phys. Conf. Ser. **161**, 012015 (2009).
[30] I. Cavero-Peláez, K. A. Milton, P. Parashar, and K. V. Shajesh, Phys. Rev. D **78**, 065019 (2008).
[31] L. H. Ford and N. F. Svaiter, Phys. Rev. A **62**, 062105 (2000).